Mater. Res. Soc. Symp. Proc. Vol. 1060 © 2008 Materials Research Society 1060-LL05-07

Elasticity Models for the Spherical Indentation of Gels and Soft Biological Tissues

David C. Lin, Emilios K. Dimitriadis, and Ferenc Horkay
National Institutes of Health, Bethesda, MD, 20892

ABSTRACT

AFM micro- or nanoindentation is a powerful technique for mapping the elasticity of materials at high resolution. When applied to soft matter, however, its accuracy is equivocal. The sources of the uncertainty can be methodological or analytical in nature. In this paper, we address the lack of practicable nonlinear elastic contact models, which frequently compels the use of Hertzian models in analyzing force curves. We derive and compare approximate force-indentation relations based on a number of hyperelastic general strain energy functions. These models were applied to existing data from the spherical indentation of native mouse cartilage tissue as well as chemically crosslinked poly(vinyl alcohol) gels. For the biological tissue, the Fung and single-term Ogden models were found to provide the best fit of the data while the Mooney-Rivlin and van der Waals models were most suitable for the synthetic gels. The other models (neo-Hookean, two-term reduced polynomial, Fung, van der Waals, and Hertz) were effective to varying degrees. The Hertz model proved to be acceptable for the synthetic gels at small strains (<20% for the samples tested). Although this finding supports the generally accepted view that many soft elastic materials can be assumed to be linear elastic at small strains, we propose the use of the nonlinear models when evaluating the large-strain indentation response of gels and tissues.

INTRODUCTION

In numerical simulations or uniaxial and biaxial mechanical tests, polymer gels and biological tissues are often modeled successfully using linear elasticity theory at small strains and rubber elasticity theory at large strains. For measurement of elasticity at micron and submicron length scales, the prevalence of atomic force microscopy in materials research has established nanoindentation as one of the leading techniques. However, despite advancements in instrumentation and analysis methods, its application to soft matter is still complicated by tip-sample interactions and the lack of practical nonlinear contact mechanics models. Many investigators rely on models based on the Hertz theory to analyze force curves. Consequently, errors are frequently incurred by applying these linear elastic representations beyond their validity range or at the small-strain range where the indentation process is most prone to noise.

We have developed approximate relations for the non-interactive, spherical indentation of non-Hookean materials. From the Hertz equation and various strain energy functions, force-indentation relationships were formulated in the following forms: neo-Hookean [1], Mooney-Rivlin [1], two-term reduced polynomial [2], single-term Ogden [3], Fung [4,5], and van der Waals [6]. In this paper, we first introduce these contact mechanics equations. Results of testing each model by fitting it to data obtained from the large-strain indentation of swollen poly(vinyl alcohol) gels and of native cartilage samples are then presented. Limiting the number of fitting parameters in each equation to two, we identify those models that were found to be most suitable for rubber-like gels and biological extracellular matrices and cells.

THEORY

Strain energy potentials, uniaxial stress-strain relationships, and the derived force-indentation equations are listed in Table I. The derivation approach has been described elsewhere [7] and will only be briefly summarized here. We define the indentation stress ($\sigma^* = F / \pi a^2$, where F is the force applied to the indenter and a the contact radius) and strain ($\varepsilon^* = a / R$, where R is the radius of the indenter) such that they are linearly proportional for Hertzian contact. The uniaxial stress-strain relations are then transformed into force-indentation equations by assuming that the contact radius varies with indentation depth (δ) in the Hertzian manner. Tip-sample interactions are assumed to be negligible.

Table I. Strain energy potentials and the stress-strain and contact equations derived from them.

Name	**Strain energy potential (W)** **Uniaxial stress (σ) – stretch (λ) equation** **Force (F) – indentation (δ) equation** (FP: fitting parameters; E is initial/ infinitesimal Young's modulus)
Mooney-Rivlin Neo-Hookean [1]	$W_{MR} = \boldsymbol{C}_1(I_1 - 3) + \boldsymbol{C}_2(I_2 - 3)$; $\sigma = 2\boldsymbol{C}_1(\lambda - \lambda^{-2}) + 2\boldsymbol{C}_2(1 - \lambda^{-3})$ $F = \pi R^{1/2}\boldsymbol{B}_1\left(\frac{\delta^{5/2} - 3R^{1/2}\delta^2 + 3R\delta^{3/2}}{\delta - 2R^{1/2}\delta^{1/2} + R}\right) + \pi R^{1/2}\boldsymbol{B}_2\left(\frac{R^{1/2}\delta^{5/2} - 3R\delta^2 + 3R^{3/2}\delta^{3/2}}{-\delta^{3/2} + 3R^{1/2}\delta - 3R\delta^{1/2} + R^{3/2}}\right)$; $\boldsymbol{B}_1 + \boldsymbol{B}_2 = \frac{4E}{9\pi(1-\nu^2)}$, $\boldsymbol{C}_2 = \boldsymbol{B}_2 = 0$ (neo - Hookean); FP : $\boldsymbol{B}_1, \boldsymbol{B}_2$
Reduced polynomial ($N = 2$) [2]	$W_{rp} = \sum_{i=1}^{N} \boldsymbol{C}_i(I_1 - 3)$; $\sigma = 2(\lambda - \lambda^{-2})\sum_{i=1}^{N} i\boldsymbol{C}_i(\lambda^2 + 2\lambda^{-1} - 3)^{i-1}$ $F = \pi R\delta\boldsymbol{B}_1\left[\frac{1}{(1-\varepsilon^*)^2} + \varepsilon^* - 1\right] + \pi R\delta\boldsymbol{B}_2\left[-(1-\varepsilon^*)^3 - \frac{3}{(1-\varepsilon^*)^2} + \frac{2}{(1-\varepsilon^*)^3} - 3\varepsilon^* + 2\right]$; $\boldsymbol{B}_1 = \frac{4E}{9\pi(1-\nu^2)}$; FP : $\boldsymbol{B}_1, \boldsymbol{B}_2$
Ogden ($N = 1$) [3]	$W_{Og} = \sum_{i=1}^{N} \frac{2\boldsymbol{C}_i}{\boldsymbol{\alpha}_i^2}\left(\lambda_1^{\boldsymbol{\alpha}_i} + \lambda_2^{\boldsymbol{\alpha}_i} + \lambda_3^{\boldsymbol{\alpha}_i} - 3\right)$; $\sigma = \sum_{i=1}^{N} \frac{2\boldsymbol{C}_i}{\boldsymbol{\alpha}_i}\left(\lambda^{\boldsymbol{\alpha}_i - 1} - \lambda^{-\frac{1}{2}\boldsymbol{\alpha}_i - 1}\right)$ $F = \frac{\pi R\delta\boldsymbol{B}}{\boldsymbol{\alpha}}\left[(1-\varepsilon^*)^{-\frac{1}{2}\boldsymbol{\alpha}-1} - (1-\varepsilon^*)^{\boldsymbol{\alpha}-1}\right]$; $\boldsymbol{B} = \frac{4E}{4.5\pi(1-\nu^2)}$; FP : $\boldsymbol{B}, \boldsymbol{\alpha}$
Fung [4,5]	$W_{Fu} = \frac{\boldsymbol{C}}{2\boldsymbol{b}}\{\exp[\boldsymbol{b}(I_1 - 3)] - 1\}$; $\sigma = \boldsymbol{C}(\lambda - \lambda^{-2})\exp[\boldsymbol{b}(I_1 - 3)]$ $F = \pi R^{1/2}\boldsymbol{B}\left(\frac{\delta^{5/2} - 3R^{1/2}\delta^2 + 3R\delta^{3/2}}{\delta - 2R^{1/2}\delta^{1/2} + R}\right)\exp\left[\boldsymbol{b}\left(\frac{\delta^{3/2} - 3R^{1/2}\delta}{R\delta^{1/2} - R^{3/2}}\right)\right]$; $\boldsymbol{B} = \frac{4E}{4.5\pi(1-\nu^2)}$ FP : $\boldsymbol{B}_1, \boldsymbol{b}$

(cont'd)

Table I (cont'd)

Van der Waals (Kilian) [6]	$W_{vdW} = \boldsymbol{C}\left\{-(I_{1m}-3)\left[\ln\left(1-\sqrt{\frac{I_1-3}{I_{1m}-3}}\right)+\sqrt{\frac{I_1-3}{I_{1m}-3}}\right]-\frac{2}{3}\boldsymbol{a}\left(\frac{I_1-3}{2}\right)^{3/2}\right\}$ $\sigma = \boldsymbol{C}(\lambda-\lambda^{-2})\left[\left(1-\sqrt{\frac{\lambda^2+2\lambda^{-1}-3}{\lambda_m^2+2\lambda_m^{-1}-3}}\right)^{-1}-\boldsymbol{a}\sqrt{\frac{\lambda^2+2\lambda^{-1}-3}{2}}\right]$ $F = \pi R^{1/2}\boldsymbol{B}\left(\frac{\delta^{5/2}-3R^{1/2}\delta^2+3R\delta^{3/2}}{\delta-2R^{1/2}\delta^{1/2}+R}\right)\left[\left(1-\sqrt{\frac{(\varepsilon^*)^3-3(\varepsilon^*)^2}{1-\varepsilon^*}\frac{1-\varepsilon^*_m}{(\varepsilon^*_m)^3-3(\varepsilon^*_m)^2}}\right)^{-1}-\boldsymbol{a}\sqrt{\frac{-(\varepsilon^*)^3+3(\varepsilon^*)^2}{2(1-\varepsilon^*)}}\right]$; $\boldsymbol{B} = \frac{4E}{4.5\pi(1-\nu^2)}$; FP : $\boldsymbol{B},\boldsymbol{a}$

Notes:

i. Hertz equation: $F = 4ER^{1/2}\delta^{3/2}[3(1-\nu^2)]^{-1}$ where R is the radius of the spherical tip and ν is Poisson's ratio.
ii. Elastic constants ($\boldsymbol{C}$) in the potential and σ-λ equations are replaced by $\boldsymbol{B}$ in the F-δ equations.
iii. Stretch ratios in the three principal directions are represented by λ_i, i = 1, 2, 3.
iv. I_1 is the first strain invariant: $I_1 = \lambda_1 + \lambda_2 + \lambda_3$; I_2 is the second invariant: $I_2 = \lambda_1^{-2} + \lambda_2^{-2} + \lambda_3^{-2}$ for incompressible materials.
v. Under uniaxial loading in the 1-direction, $\lambda_1 = \lambda$ and $\lambda_2 = \lambda_3 = \lambda^{-1/2}$.
vi. The fitting parameters α in the Ogden model and $\boldsymbol{b}$ in the Fung model are nondimensional.
vii. In the van der Waals model, $\boldsymbol{a}$ is the global interaction parameter between network chains. I_{1m} is the limiting value of I_1. Under uniaxial loading, $I_{1m} = \lambda_m + 2/\lambda_m$, where λ_m is the maximum stretch ratio (limited by finite chain extensibility).
viii. $\varepsilon^*_m = 1$ is the limiting value of the indentation strain ε^*.

EXPERIMENT

Macroscopic compression and AFM micro-indentation of chemically crosslinked poly(vinyl alcohol) gels have been described elsewhere [8]. We cast gel cylinders (1 cm diameter, 1 cm height) and films (> 2 mm thick) for macroscopic displacement-controlled compression and AFM nanoindentation, respectively. Sixty-micrometer thick cartilage samples were transversely sectioned from the femoral heads of one-day old wild-type mice using a microtome. Samples were lightly fixed in formaldehyde and frozen in embedding matrix prior to sectioning.

General-purpose silicon nitride tips with 5.5 μm glass (for the synthetic gels) or 5 μm polystyrene (for cartilage) beads attached were used for the AFM measurements, performed using a commercial AFM (Bioscope I with Nanoscope IV controller, Veeco). The spring constant of the cantilever was measured by the thermal tune method while bead diameters were measured from images acquired during the attachment process. A raster scanning approach ("force-volume") was applied to automatically perform indentations over an area of ~ 30×30 μm, at a resolution of 16×16 (256 total indentations) for the hydrogel and 32×32 (1024 indentations) for the cartilage. Code written in Matlab was used to automatically process each dataset and extract values of Young's modulus. For the cartilage, height images were used to determine whether each measurement location corresponded to the extracellular matrix or to the cells.

RESULTS AND DISCUSSION

Ten random indentations were selected from the force-volume scan of the poly(vinyl alcohol) gel for processing using the different force-indentation equations in Table I. From the scan of the cartilage, ten indentations each of the matrix and cells were chosen. Mean square errors and extracted Young's moduli are listed in Table II. Two representative fits for the synthetic gel are shown in Figure 1. Likewise, representative fits for the cartilage extracellular matrix are presented in Figure 2 along with a sample AFM height image.

Chemically crosslinked poly(vinyl alcohol) gels swollen in water are known to be rubber-like in their deformation behavior [9]. It is therefore not unexpected that many of the rubber elasticity models produced good fits of the data, as indicated by the mean square errors in Table II. Limiting the Hertzian analysis to different levels of indentation strain revealed a linear elastic limit of between 20% and 25%. When sufficient points are retained in the truncated data sets, this is a viable approach for determining Young's modulus. Among the hyperelastic theories, our results show the Mooney-Rivlin, reduced polynomial, Fung, and van der Waals models to be best.

In the cartilage data, the poor fits with the Hertz equation even at limited strains of about 15% suggested a much narrower linear regime. Further truncation of the data sets was not attempted due to the lack of sufficient data points. As anticipated, the van der Waals model, which aims to account for network effects such as finite chain extensibility [5], also results in poor fits of the cartilage data. The cellular cytoplasm and the collagen network structure of the extracellular matrix differ significantly from crosslinked polymer networks of flexible chains on which these particular models are based.

Among the phenomenological theories of large strain, elastic deformations, the Fung and Ogden models have been applied successfully to a number of soft tissues (e.g., muscle and skin [4], arteries [5], and brain [10]). The results of this study provide further validity to the effectiveness of those models in describing the hyperelastic behavior of many soft biological materials. We attribute the discrepancy in the elastic moduli obtained using the two force-indentation relationships (Table II) to the retention of only a single term in the Ogden model. The inclusion of more terms would increase the number of fitting parameters and yield solutions that are no longer unique. Since the Fung model is already in closed form and contains two fitting parameters, we submit that it is preferable to the Ogden model.

Due in large part to differences in technique, interpretation and modeling of test data, source and condition of samples, and developmental state of the samples, values of elastic moduli reported in the literature for chondrocytes, matrix, and bulk cartilage vary over a large range; comparison is therefore difficult. Noting that the stiffness of the samples used in this study were possibly altered by the chemical fixation process, the elastic modulus of the matrix using the Fung model compare most favorable with the results of Guilak et al [11], who found for the pericellular matrix from the middle zone of the canine knee, $E = 23.2 \pm 7.1$ kPa. The elastic moduli of the chondrocytes compare most favorably with the instantaneous values reported by Koay et al [12], $E = 8.0 \pm 4.41$ kPa.

Table II. Comparison of models' ability to fit experimental, hyperelastic force curves.

	PVA, n = 10, R = 4.8 μm		Chondrocytes, n = 10		Cartilage Matrix, n = 10	
	E (kPa)*	MSE (nm^2)	E (kPa)*	MSE (nm^2)	E (kPa)*	MSE (nm^2)
mc	~20	-	-	-	-	-
Hz	22.76 ± 0.85	0.465	60.57 ± 17.93	23.19	132.31 ± 33.33	25.58
Hz-s	19.62 ± 1.16	0.168	22.49 ± 7.40	0.515	93.94 ± 54.24	10.99
nH	15.40 ± 0.99	0.493	33.92 ± 13.35	13.77	93.08 ± 30.21	16.85
MR	17.35 ± 1.40	0.193	21.41 ± 7.49	10.05	67.01 ± 22.63	13.22
rp	16.62 ± 1.14	0.219	6.12 ± 2.26	0.393	1.93 ± 2.51	0.836
Og	15.85 ± 0.97	0.497	14.30 ± 2.44	0.138	23.21 ± 2.05	0.133
Fu	16.65 ± 1.15	0.218	11.81 ± 1.76	0.125	19.83 ± 1.67	0.138
vdW	17.57 ± 1.48	0.208	31.27 ± 12.51	12.83	84.87 ± 29.60	16.24

* Mean ± standard deviation

MSE (mean square error), mc (macroscopic compression), Hz (Hertz), Hz-s (Hertz, small strain), nH (neo-Hookean), MR (Mooney-Rivlin), rp (reduced polynomial), Og (Ogden), Fu (Fung), vdW (van der Waals)

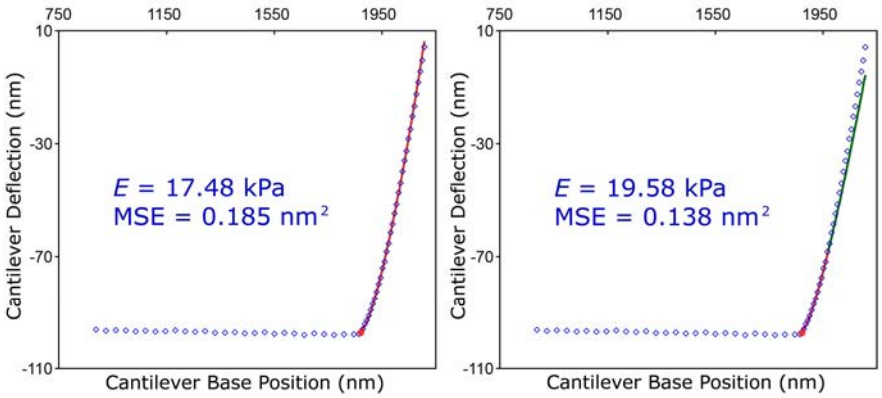

Figure 1. Representative full fit (left, Mooney-Rivlin model) and Hertzian fit (right) of a sample dataset from the indentation of the poly(vinyl alcohol) gel. Approximately 20% of data points are plotted; the best-fit curves and contact points are shown in red. For the Hertz fit, analysis was limited to 15% strain. The green curve represents the fit extended to the remainder of the data and clearly shows that the Hertz theory does not account for the stiffening that occurs.

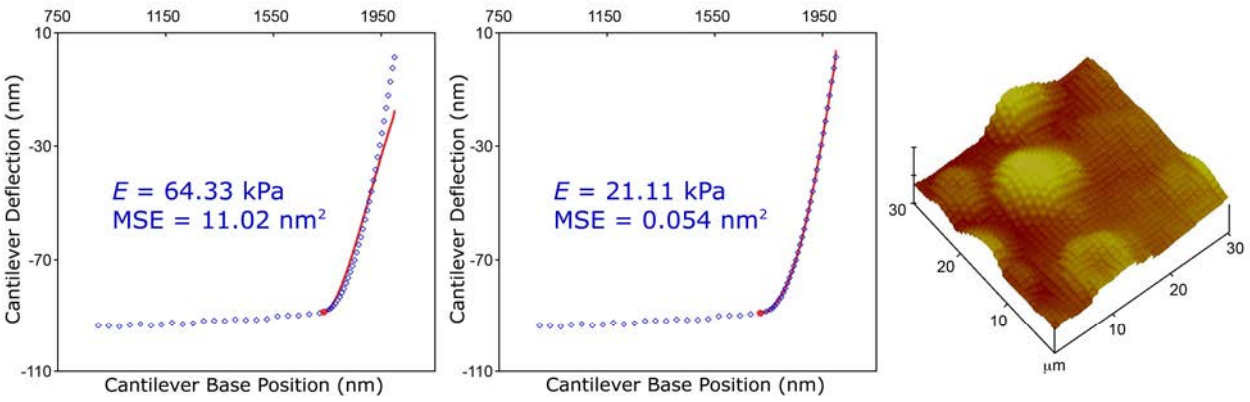

Figure 2. Representative poor fit (left, Mooney-Rivlin model) and good fit (center, Fung model) of a sample dataset from the indentation of cartilage matrix. Approximately 20% of data points are plotted; the best-fit curves and contact points are shown in red. The image on the right is a height scan of the region, with cells clearly visible.

CONCLUSIONS

The prevalence of nanoindentation in measuring the local elastic properties of a wide range of materials necessitates the development of contact models that accurately represent various material behaviors. Simple force-indentation relationships are especially desirable for automated and high-throughput applications. The contact equations presented here should satisfy a broad range of nonlinearly elastic soft materials, from rubber-like gels to biological tissues and cells. As this study has shown, extreme caution should be exercised when selecting an appropriate hyperelastic model in order to avoid potentially large errors.

ACKNOWLEDGMENTS

This work was supported by the Intramural Research Program of the NIH/NICHD. The authors would like to thank Ed Mertz for assisting in the preparation of the cartilage samples.

REFERENCES

1. L.R.G. Treloar, *The Physics of Rubber Elasticity*, 3rd ed (Oxford University Press, Oxford, 1975).
2. M. Mooney, J. Appl. Phys. **11**, 582 (1940).
3. R.W. Ogden, Proc. R. Soc. Lond. A **328**, 567 (1972).
4. Y.C. Fung, Am. J. Physiol. **213**, 1532 (1967).
5. Y.C. Fung, K. Fronek, P. Patitucci, Am. J. Physiol. **237**, H620 (1979).
6. H.G. Kilian, Colloid Polym. Sci. **263**, 30 (1985).
7. D.C. Lin, E.K. Dimitriadis, F. Horkay, eXPRESS Polym. Lett., **1**, 576 (2007).
8. D.C. Lin, E.K. Dimitriadis, F. Horkay, J. Biomech. Eng. **129**, 430 (2007).
9. G.B. McKenna, F. Horkay, Polymer **35**, 5737 (1994).
10. M.T. Prange, S.S. Margulies, J. Biomech. Eng. **124**, 244 (2002).
11. F. Guilak, L.G. Alexopoulos, M.A. Haider, H.P. Ting-Beall, L.A. Setton, Ann. Biomed. Eng. **33**, 1312 (2005).
12. E.J. Koay, A.C. Shieh, K.A. Althanasiou, J. Biomech. Eng. **125**, 334 (2003).